Journal of Power Sources xxx (xxxx) 238850

Contents lists available at ScienceDirect

Journal of Power Sources

journal homepage: www.elsevier.com/locate/jpowsour

Etching-assisted upcycling of Ni-lean to Ni-rich cathode materials

Zifei Meng [a], Xiaotu Ma [a, b], Jiahui Hou [a], Hao Zhou [a], Zexin Wang [a], Zeyi Yao [a], Wenting Jin [a], Jinzhao Fu [a], Zhenzhen Yang [c], Adam Shenk [a], Yifan Zhang [a], Yu Zhong [a], Yan Wang [a, *]

[a] Department of Mechanical and Materials Engineering, Worcester Polytechnic Institute, 100 Institute Road, Worcester, MA, 01609, USA
[b] The School of Systems Science and Industrial Engineering, Binghamton University, 4400 Vestal Pkwy E, Binghamton, NY, 13902, USA
[c] Chemical Sciences and Engineering Division, Argonne National Laboratory, Lemont, IL, 60439, USA

ARTICLE INFO

Keywords:
Upcycling
Enhanced sustainability
High energy density
Acid etching
Single crystal cathodes

ABSTRACT

Upcycling is recognized as a sustainable recycling approach for spent lithium-ion batteries. However, existing upcycling methods typically involve intricate pretreatment or post-treatment steps, complicating their practical application. Here, we propose a straightforward, etching-assisted upcycling method that effectively transforms polycrystalline Ni-lean cathodes into high-performance single crystal Ni-rich cathodes. During the etching step, nickel acetate was dissolved into acetic acid and then polycrystalline NMC111 are etched in the solution. Finally, polycrystalline NMC111 are converted into single crystal particles coated with amorphous nickel acetate. This significantly enhances elemental diffusion during subsequent sintering by minimizing both particle size and the contact distance between NMC111 and nickel acetate. As elemental diffusion is improved and acetate ions decompose completely during sintering, the process requires neither additional pretreatment nor post-treatment. The resulting cathode materials (Etched-UP622) exhibit superior structural and electrochemical properties compared to the Control622, achieving an energy density of 719.7 Wh/kg, approximately 56.7 mAh/g higher than Control622 and 125.5 Wh/kg higher than NMC111. Etched-UP622 also delivers higher discharge capacity, improved rate performance and cycling stability, surpassing Control622 and NMC111. Meanwhile, NMC811 also can be synthesized by the proposed strategy, and the discharge capacity can reach 166.9 mAh/g at 1C, ~14 mAh/g higher than Control811. Overall, this etching-assisted strategy simplifies the upcycling process and offers a scalable, sustainable route for producing high-quality cathode materials.

1. Introduction

Lithium-ion batteries (LIBs) have become the dominant energy storage solution for various applications, particularly electric vehicles (EVs). However, the typical lifespan of LIBs in EVs is approximately 8–10 years, resulting in an exponential increase in the number of spent LIBs which require effective recycling [1–3]. Consequently, the global LIB recycling market has expanded rapidly, valued at approximately $4.97 billion in 2023, and is projected to reach $17.67 billion by 2029 [4]. Efficient recycling of spent LIBs is thus critical for both environment and resource recovery. Among the different components of LIBs, the cathode significantly affects the battery's performance, particularly its energy density [4,5]. $LiNi_{1-x-y}Mn_xCo_yO_2$(NMC) cathodes are the most common cathode materials due to their superior electrochemical properties [6]. Therefore, various methods have been developed to recycle NMC cathodes and the main recycling processes include pyrometallurgical, hydrometallurgical, and direct recycling methods [7–11]. Compared to pyrometallurgical and hydrometallurgical processes, direct recycling provides notable advantages by restoring cathode materials to their original performance characteristics without complete chemical decomposition [12,13]. This results in significantly reduced wastewater generation, lower energy consumption, and simplified recycling processes, making direct recycling a highly attractive option [14,15].

Despite the advantages offered by direct recycling methods, continuous advancements in cathode chemistry necessitate further innovations in recycling technologies [16]. However, the recovered NMC111 only can deliver low energy density, limiting the utilization for next generation applications which require high energy density. Meanwhile, market demands increasingly favor high-nickel NMC cathodes due to their enhanced energy densities, driving research efforts towards upcycling strategies that can convert Ni-lean into Ni-rich cathodes [17–20]. A critical aspect of successful cathode upcycling is achieving uniform elemental diffusion, particularly nickel ions [21]. Among the existing upcycling strategies, several approaches have been applied to optimize

* Corresponding author.
E-mail address: yanwang@wpi.edu (Y. Wang).

https://doi.org/10.1016/j.jpowsour.2025.238850
Received 6 August 2025; Received in revised form 27 October 2025; Accepted 12 November 2025
0378-7753/

the diffusion of nickel ions: molten salt sintering (creating a liquid environment at low temperature), precipitation (growing nickel source on the surface of $LiNi_{0.33}Mn_{0.33}Co_{0.33}O_2$ (NMC111)), and ball milling (reducing the particle size to short the diffusion path). Among the existing upcycling strategies, molten salt methods have shown particular effectiveness by creating high-temperature liquid environments that significantly enhance the diffusion rates of nickel ions [19,22]. For example, Ma et al. upcycled polycrystalline (PC) NMC111 to single crystal (SC) $LiNi_{0.6}Mn_{0.2}Co_{0.2}O_2$ (NMC622) by adding excess of LiOH and Li_2SO_4 as molten salts [22]. After sintering, ball milling and washing, upcycled NMC622 was obtained. However, the introduction of molten salts and excess lithium can induce severe particle agglomeration. Consequently, additional ball milling and washing steps are necessary to disperse the agglomerates and eliminate residual salts, thereby increasing the process complexity and leading to the waste of excess lithium salts. To improve the metal ions diffusion without molten salts, growing nickel salt on the surface of NMC is also an effective approach [23]. Allen et al. added NMC111 into a coprecipitation reactor and allowed $Ni(OH)_2$ to grow on the surface of NMC111 by pumping into $NiSO_4$ and NaOH with high-speed stirring [23]. The obtained precursor was sintered to obtain the upcycled NMC622 [23]. However, this process consumes a large volume of solution during the coprecipitation reaction. Moreover, the significant residual lithium remaining on the surface of the upcycled NMC622 necessitates additional washing and annealing steps, which not only generate wastewater but also increase the complexity of post-treatment procedures. Overall, these established methods typically require post-treatments, like washing and annealing, to remove residual molten salts and excess lithium as well as recovery structure, leading to wastewater generation, increased complexity, and higher costs.

To prevent the post-treatment and improve the elemental diffusion, ball milling was used to reduce the particle size of NMC111 which can enhance the diffusion of nickel ions by reducing the diffusion path. Zhang et al. developed a pretreatment process involving ball milling of NMC111 to reduce particle size, followed by a pre-oxidation step to improve the contact between NMC111 and nickel salts. After the pretreatment, the powder was mixed with lithium salts and sintered at high temperature to synthesize NMC622 [24]. However, the complex pretreatment and multistep sintering procedures result in high energy consumption and increased process complexity. To avoid multistep sintering, Gao et al. pelletized the mixture of NMC111 and Ni sources after ball milling, which optimized the interfacial contact and enhanced Ni ions diffusion during high-temperature sintering [25]. Nevertheless, the pelleting process is difficult to scale up, and the pretreatment remains complicated because it involves both ball milling and pelletizing. Although ball milling effectively reduces particle size and shortens the diffusion path, additional pretreatment steps such as pre-oxidation and pelletizing are still required to improve the contact between nickel salts and NMC111, leading to complex processing and limited scalability. Therefore, reducing particle size and improving the contact of NMC and Ni salts with simple processes to enhance the Ni and Li diffusion during high temperature sintering is still the challenge for upcycling Ni-lean to Ni-rich cathode materials.

Herein, we introduce an innovative etching-assisted upcycling method which can reduce the diffusion path by transferring PC NMC111 to SC NMC111 and improving the contact of NMC and Ni salts by precipitating nickel acetate on the NMC111 particles only in one step, facilitating effective diffusion during subsequent sintering. Meanwhile, the acetate ions can be burnt out during sintering, without requiring additional washing step. This simplified method successfully synthesizes the upcycled NMC622 cathode (Etched-UP622) with well layer structure, homogeneous element distribution and excellent electrochemical performance. Notably, the energy density of Etched-UP622 can reach 719.7 Wh/kg, 56.7 Wh/kg higher than that of commercial NMC622 cathodes (Control622) and 125.5 Wh/kg higher than that of NMC111. Meanwhile, Etched-UP622 also demonstrates a high specific discharge capacity of 188.3 mAh/g, outperforming Control622 by 13 mAh/g and NMC111 by 31 mAh/g. Additionally, this method exhibits versatility, effectively upcycling NMC111 to higher nickel-content NMC811 cathodes, thereby aligning with evolving market demands for advanced, high-energy-density cathode materials.

2. Experimental section

2.1. Materials preparation

2.1.1. Synthesize Etched-UP622

To increase the content of nickel, nickel acetate ($Ni(AC)_2$) was employed as nickel source and stoichiometric $Ni(AC)_2$ was dissolved into 0.5 M acetic acid. When the $Ni(AC)_2$ was fully dissolved, PC NMC111 was added in the solution with a solid to liquid ratio of 1/20 and etched at room temperature. After 25 h, the temperature was increased to 50 °C to evaporate the excess acetic acid, and the dried SC NMC111 covered with $Ni(AC)_2$ was obtained. The dried etched powders were mixed with $LiOH{\cdot}H_2O$ to make the Li content to 1.05 M ratio, and the mixture was sintered 450 °C for 5 h and 950 °C for 12 h under oxygen atmosphere to obtain Etched-UP622.

2.1.2. Synthesize Etched-UP811

To increase the content of nickel, nickel acetate ($Ni(AC)_2$) was employed as nickel source and stoichiometric $Ni(AC)_2$ was dissolved into 0.5 M acetic acid. When the $Ni(AC)_2$ was fully dissolved, PC NMC111 was added in the solution with a solid to liquid ratio of 1/35 and etched at room temperature. After 25 h, the temperature was increased to 50 °C to evaporate the excess acetic acid, and the dried SC NMC111 covered with $Ni(AC)_2$ was obtained. The dried etched powders were mixed with $LiOH{\cdot}H_2O$ to make the Li content to 1.05 M ratio, and the mixture was sintered 450 °C for 5 h and 850 °C for 18 h under oxygen atmosphere to obtain Etched-UP622.

2.2. Characterization methods

X-ray diffraction (XRD) patterns were collected using a PANalytical Empyrean diffractometer with Cu Kα radiation (λ = 1.5409 Å, step size = 0.0167°). Rietveld refinements were conducted using FullProf Suite. Surface morphology and elemental mapping were examined via scanning electron microscopy (SEM) and energy-dispersive X-ray spectroscopy (EDS) using a JEOL JSM-7000F SEM at 10 kV. Focused ion beam (FIB) and cross-section SEM were using Thermo Scientific Scios 2 DualBeam system. Inductively coupled plasma optical emission spectrometry (ICP-OES) was used to determine Chemical compositions. Surface chemical states and depth profiles were characterized using X-ray photoelectron spectroscopy (XPS) with a PHI 5000 VersaProbe II (Al Kα, 1486.6 eV). High-resolution spectra were acquired at a pass energy of 23.5 eV, and survey scans at 117.4 eV C1s (284.8 eV) was used as a reference for charge correction. Data were analyzed with Shirley background subtraction and peak fitting using Gaussian-Lorentzian functions in XPSpeak 41. Simultaneous Thermal Analyzer (SDT Q600-TA Instruments) was used to study the thermal behavior during sintering.

2.2.1. Electrode/half-cell fabrication

Cathodes were fabricated by mixing active material, Super C65 carbon black (conductive agent), and PVDF binder in NMP at a weight ratio of 80:10:10. The slurry was coated onto 15 μm thick Al foil using a 150 μm doctor blade and initially dried at 105 °C under vacuum. The loading mass of active material was controlled to ~4.5 mg/cm^2. The electrodes were then dried overnight at 120 °C to eliminate residual solvents. The dried films were calendared to 35–40 μm, punched into 12 mm discs, and assembled into CR2032 coin cells in an argon-filled glovebox, using lithium metal as the anode, 1.0 M $LiPF_6$ in EC/DMC (3:7 w/w) as the electrolyte, and Celgard separator.

Electrochemical performance was tested using a LANDT CT2001A system. Initial charge/discharge profiles were measured at 0.05 C (2.5–4.3 V vs. Li/Li^+). Rate capability was assessed by cycling at increasing rates of 0.05, 0.1, 0.2, 0.5, 1.0, 2.0, 3.0, and 5.0 C. Cycling stability was evaluated at 2 C within the same voltage window. All the testing is under room temperature. EIS was tested by a 10 mV sinusoidal amplitude between 1 MHz and 20 mHz.

The CV curves are tested at 0.1, 0.4, 0.7, 1.0, and 1.3 mV/s between 2.8 and 4.6V. The lithium ions diffusion coefficient can be calculated by Randles–Sevcik equation: $I_p^2 = \left(2.69 \times 10^5\right)^2 n^3 A^2 D_{L_i} C^2 v$, where the number of electrons transferred in the redox reaction (n = 1); A is electrode surface area (1.13 cm^2); C is the theoretical molar concentration of lithium ions in the NMC crystal (0.05 mol/cm^3); and D_{Li} is the lithium ions diffusion coefficient. D_{Li} can be calculated by the slope of the linear relationship of Ip2 vs υ.

3. Results and discussion

3.1. Etching process for NMC111 cathode materials

In the etching-assisted upcycling strategy, the etching process simultaneously reduces the particle size and precipitates $Ni(AC)_2$ onto NMC particles in a single step (Fig. 1). During etching, PC NMC111 was transferred to SC NMC111, significantly reducing the particle size. Meanwhile, $Ni(AC)_2$, which exhibits high solubility in acetic acid, can serves as a suitable nickel precursor for NMC synthesis [26]. During the evaporation step, $Ni(AC)_2$ can precipitate on the surface of single crystal NMC111. Upon high-temperature sintering, $Ni(AC)_2$ can decompose into NiO, CO_2 and H_2O, leaving no impurity residues [27].Therefore, $Ni(AC)_2$ is selected as the nickel source in this process. $Ni(AC)_2$ is initially dissolved within the etching solution and subsequently precipitated onto SC NMC111, enabling close contact between NMC and $Ni(AC)_2$ and allowing Ni to directly diffuse from the surface to the bulk of NMC111 during high temperature sintering. Due to the optimized diffusion path and close contact between particles, pretreatment and extra molten salts are not required to further enhance the diffusion of Ni. Additionally, $Ni(AC)_2$ can be decomposed to NiO, H_2O, and CO_2 at high temperature, without introducing impurities [28]. Thus, post-treatments, like washing and annealing, are not required. Therefore, by applying etching process and $Ni(AC)_2$, the process of upcycling NMC can be simplified to two steps.

To elucidate the mechanisms of the etching process, PC NMC111 was treated for various durations. It was observed that increasing etching time progressively transformed PC NMC111 into single-crystal particles, with complete conversion achieved after 25 h (Fig. 2a). Meanwhile, the structure of NMC111 was also changed during etching, which was investigated by XRD (Fig. S1). The (003) peak shifted toward lower angles, reflecting expansion along the c-axis [29]. The clearly distinguished splitting of the (018)/(110) diffraction peaks was consistent with lithium extraction during charging processes [29]. Notably, the absence of (104)/(101) peak splitting indicated no monoclinic distortion, confirming the maintained layered structure [29]. Thus, the etching strategy effectively transforms PC NMC111 into single crystal particles to reduce the diffusion path and promote beneficial lattice expansion without destroying the layer structure of NMC111. Meanwhile, the roles of acid corrosion and high-speed stirring on the transformation from polycrystal NMC111 to single crystal NMC111 are analyzed. As shown in Fig. S2, when the PC NMC111 was etched with water at high-speed stirring, only small number of secondary particles can transfer to SC NMC111, indicating the importance of the grain boundary corrosion by acetic acid. When the PC NMC111 was etched with acetic acid at low speed stirring, only lots of secondary particles can be observed, indicating the importance of high stirring speed. Therefore, PC NMC111 can be broken into SC NMC111only when combining acid corrosion and high-speed stirring.

To further study the etching process, the dissolving rate and percentage of Li, Co, Mn, and Ni from polycrystalline NMC111 into solution are investigated. During etching process, some metal ions are dissolved from NMC111 particles into solution. As shown in Fig. S3, the dissolving rate of Li is much higher than that of Ni, Mn, and Co while the dissolving rate of Ni, Mn, and Co are comparable. Specifically, the dissolving rate of Li from polycrystalline NMC111 is 124 mg/L/hour while the dissolving rate of Ni, Mn, and Co in polycrystalline NMC111 are ~70 mg/L/hour. Meanwhile, according to XRD (Fig. S1), the splitting of (018)/(110) planes are extended, which is due to the dissolving of Li from the Li layer [29].

Meanwhile, etching process also can facilitate close particle contact between NMC111 and $Ni(AC)_2$ prior to sintering, markedly reducing diffusion paths (Fig. 1). The precipitation of $Ni(AC)_2$ is investigated by ICP. As shown in Fig. S4, during precipitation, the precipitation rate of Ni (60 mg/h) is higher than other metals (~0.5 mg/h) due to the high concentration in the solution (extra Ni salts are dissolved into the solution before etching process) from 0.5 h to 1 h. After 1 h, since large number of solutions are evaporated, the concentration of Li, Ni, Mn and Co are high in the solution and the precipitation rate of Ni further increased to 393 mg/h and that of Li, Mn and Co are increased to ~3 mg/h.

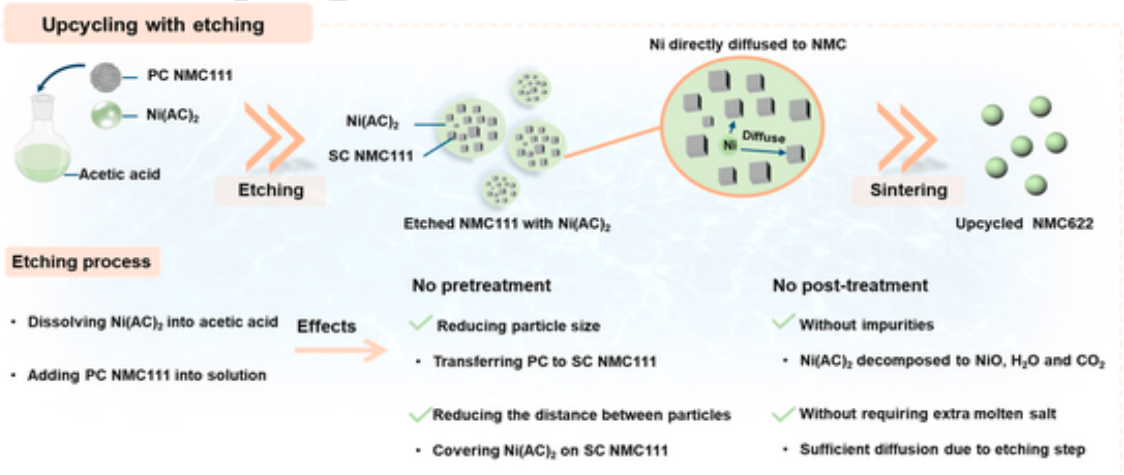

Fig. 1. Schematic for the mechanism of Ni diffusion in Etched NMC111 with $Ni(AC)_2$.

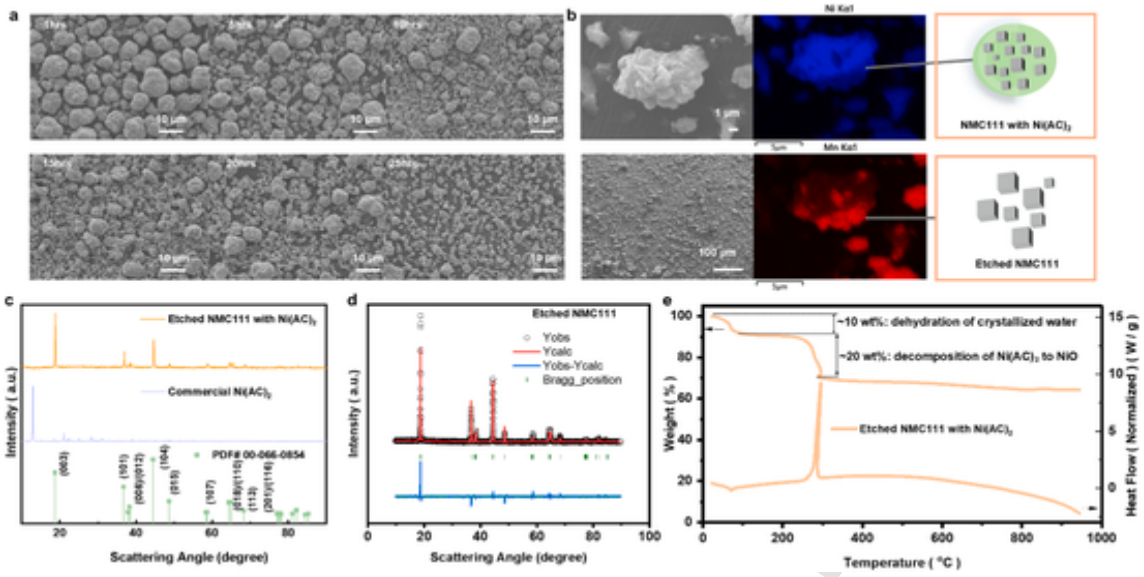

Fig. 2. Properties of Etched NMC111 with $Ni(AC)_2$. a) SEM of etched NMC111 with different etching time. b) SEM and EDS mapping of Etched NMC111 with $Ni(AC)_2$. c) XRD pattern of commercial $Ni(AC)_2$ and Etched NMC111 with $Ni(AC)_2$. d) XRD refinemet of Etched NMC111. e) TGA for Etched NMC111 with $Ni(AC)_2$.

The results of SEM and EDS mapping confirmed that etched samples comprised closely contacted particles covered by $Ni(AC)_2$ (Fig. 2b and Fig. S5) since Ni can be observed in the whole particle while Mn and Co only can be observed in some small parts of the particle. Additionally, the crystalline state of $Ni(AC)_2$ was altered during the etching process. XRD analysis (Fig. 2c) indicated that etched NMC111 with $Ni(AC)_2$ exhibited solely NMC111 peaks and there are no peaks for $Ni(AC)_2$. This result suggested a transformation of $Ni(AC)_2$ from crystalline to amorphous form during etching. Meanwhile, according to the XRD refinement results in Fig. 2d, Fig. S6, and Table S1, the etched NMC111 delivered larger c-axis parameter and higher cation mixing than unetched NMC111, and the cation mixing can be subsequently reduced during post-sintering. TGA and DTA provided insights into thermal behavior of etched NMC111 with $Ni(AC)_2$ during high temperature sintering (Fig. 2e). The first mass loss is around 100 °C, which is corresponding to the dehydration of crystallized water in $LiOH{\cdot}H_2O$ and $Ni(AC)_2$ [27]. Then more mass loss is around 300 °C when $Ni(AC)_2$ was decomposed to NiO [27]. According to the decomposition temperature is the same as $Ni(AC)_2$, the amorphous nickel salts in etched NMC111 can be recognized as $Ni(AC)_2$ [27]. Consequently, the etching process can effectively reduce the particle size of NMC111 and allow $Ni(AC)_2$ to be covered on NMC111, shortening the diffusion path of Ni and reducing the distance between $Ni(AC)_2$ and NMC111.

3.2. Upcycled cathodes

Different characterization techniques were employed to assess the physical and chemical properties of the upcycled cathode materials. The etched NMC111 with $Ni(AC)_2$ were sintered to produce upcycled NMC622 (Etched-UP622) and the equation is shown as below:

$$LiNi_{0.33}Mn_{0.33}Co_{0.33}O_2 + 0.66\ Ni(CH_3COO)_2 \cdot 4H_2O + 2.7975\ O_2 + 0.65\ LiOH \cdot H_2O = 1.65\ LiNi_{0.6}Mn_{0.2}Co_{0.2}O_2 + 2.64\ CO_2 + 5.595\ H_2O$$

The results of ICP confirmed successful stoichiometric conversion of NMC111 to NMC622 (Table S2). The structure of Etched-UP622 was analyzed by XRD. Etched-UP622 maintained a single-phase α-$NaFeO_2$ layered structure with distinct (006)/(102) peak splitting, indicative of superior layer ordering (Fig. 3a). Compared with NMC111, the (003) peak shift to lower angle, indicating the enlarged lattice parameter [30,31]. The crystal structure of Etched-UP622 and NMC111 also were investigated by the XRD refinement (Fig. 3b, Fig. S6, and Table S1). Comparison with NMC111, Etched-UP622 delivers larger lattice parameter in a and c-axis, enhancing Li^+ diffusion paths and thus promoting improved rate performance [32]. Notably, Etched-UP622 also exhibited significantly lower cation mixing (1.2 %) compared to NMC111 (4.76 %) [24].

Beyond structural improvements, the etching process also markedly impacted the morphology and elemental distribution within the upcycled cathode materials. The morphology of Eched-UP622 was investigated with SEM and Eched-UP622 are single crystal particles (Fig. 3c), indicating the beneficial role of the etching process in transforming polycrystal into single-crystal particles. Elemental distribution within the upcycled cathode materials was examined through EDS mapping. As shown in Fig. 3c and Fig. S7, Ni, Mn, Co and O distribute homogeneously in the Etched-UP622. The homogeneous element distribution is due to the small particle size and close contact of NMC111 and $Ni(AC)_2$ which allow short Ni diffusion path. To check the distribution of Ni in the bulk and surface of Etched-UP622, cross-sectional SEM, EDS, and linear scan were applied. All elements distribute homogeneously at the cross section of Etched-UP622 according to the EDS mapping (Fig. 3d).The linear scan of Ni for the cross section of Etched-UP622 also can support the homogeneous distribution of Ni according to the consistent intensity of Ni from surface to bulk (Fig. 3e).

3.3. Qualifying physical and chemical properties of upcycled cathodes

The physical and chemical properties of Etched-UP622 were compared with commercial NMC622 (Control622) to check the quality of Etched-UP622. As shown in Fig. 4a, both Etched-UP622 and Control622 exhibited a single-phase α-$NaFeO_2$ structure characterized by distinct splitting of (006)/(102) and (018)/(110) peaks, indicating excellent layered structure. According to the XRD refinement results in Figs. 3b and 4b and Table S1, Etched-UP622 delivers larger lattice parameter and lower cation mixing than Control622. According to the depth profile of XPS for Ni 2p3, Mn 2p3 and Co 2p3 (Fig. 4c–h) of Etched-UP622, they showed similar results, indicating the comparable chemical states of these elements from the surface to the bulk [3].

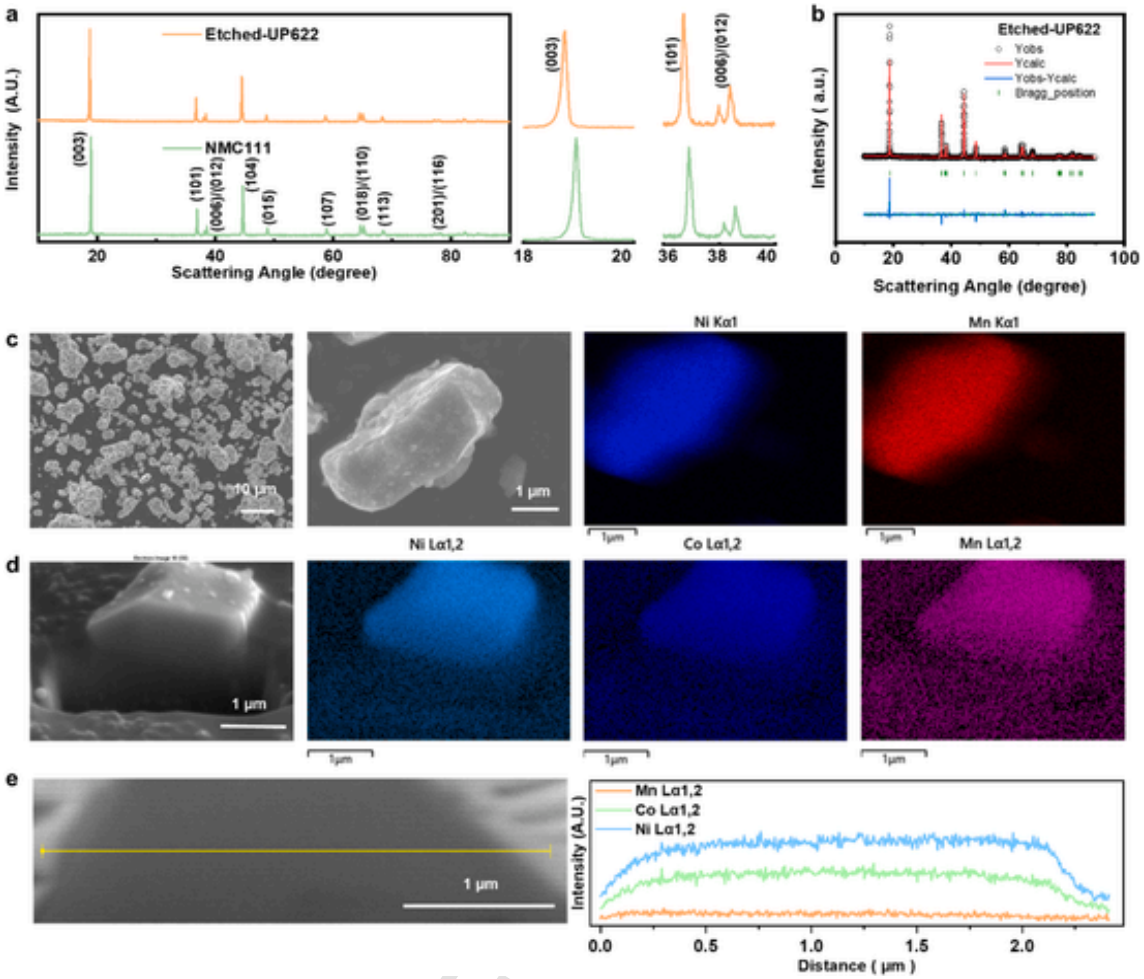

Fig. 3. Properties of Etched-UP622. a) XRD pattern of Etched-UP622. b) XRD refienment of Etched-UP622. c) SEM and EDS mapping of Etched-UP622. d) SEM and EDS mapping of the cross-section of Etched-UP622. e) linear scan of the cross-section of Etched-UP622.

However, the XPS results of Ni 2p3 in Etched-UP622 are different from that in Control622 (Fig. 4c and Fig. S8a). There are four peaks in the Ni $2p_{3/2}$ spectra, two peaks are Ni^{2+} (854 eV)and Ni^{3+} (856 eV) while the others are satellite peaks (861 and 865 eV) [33]. The percentages of Ni^{2+} in Etched-UP622 and Control622 are 32 % and 35 % respectively. Since Ni^{2+} has a similar radius to Li^+, Ni^{2+} is easier to occupy the sites of Li^+ and causes cation mixing [34]. Because Etched-UP622 contains less Ni^{2+} than Control622, Etched-UP622 delivers lower cation mixing, corresponding to the XRD refinement results. For the XPS results of Mn 2p3 and Co 2p3 (Fig. 4e–h and Fig. S8b–c) in Etched-UP622 and Control622, they deliver comparable results [3]. The XPS results of C and O for Etched-UP622 and Control622 have obvious differences. Specifically, C 1s spectra were decomposed into peaks corresponding to CO_3^{2-} (289.8 eV), C–O (286.5 eV), and C–C (284.8 eV) (Fig. 4i) [35]. Etched-UP622 demonstrated a significantly lower proportion of CO_3^{2-} (17.2 %) compared to Control622 (22.1 %), indicating that there is less Li_2CO_3 impurity on the surface of Etched-UP622 [35]. Similarly, O 1s spectra showed peaks corresponding to C-O (531.9 eV), and lattice oxygen (M – O at 530 eV) (Fig. 4j) [36]. Notably, the lattice oxygen content in Etched-UP622 was significantly higher (33.6 %) than that in Control 622 (30.5 %), suggesting less Li_2CO_3 impurity in Etched-UP622 [36,37]. Therefore, in comparison with Control622, Etched-UP622 delivered better physical and chemical properties, indicating the high quality of Etched-UP622.

3.4. Electrochemical performance of upcycled cathodes

The electrochemical performance of upcycled cathodes and commercial cathodes was tested in half cells. As shown on Fig. 5a and b, Etched-UP622 demonstrated specific capacities of 188.3 mAh/g at 0.05 C between 2.5 and 4.3V. In comparison, Control622 only achieves 175.3mAh/g, 13 mAh/g less than Etched-UP622, which is due to enlarged lattice parameter and low cation mixing of Etched-UP622. Meanwhile, NMC111 delivers 154.5 mAh/g in the initial cycle, ~34 mAh/g lower than Etched-UP622. Due to the high discharge capacity, the energy density of Etched-UP622 can reach 719.7 Wh/kg, 56.7 Wh/kg higher than that of Control622 and 125.5 Wh/kg higher than that of NMC111 (Fig. 5b). It indicates that NMC111 was successfully upcycled to NMC622 and Etched-UP622 can deliver higher specific capacity and energy density than Control622. The rate performance of Etched-UP622 is also obviously higher than Control622 and NMC111. In Fig. 5c and Table S3, Etched-UP622 delivers better rate performance than Control622 and at a high rate (5C), the specific capacity of Etched-UP622 (133.3 mAh/g) is 6.6 mAh/g higher than Control622 (126.7 mAh/g) and 14.5 mAh/g higher than NMC111(118.8 mAh/g). Meanwhile, for Etched-UP622, more than 73 % capacity can be kept when the current density changes from 0.05C to 5C, which is comparable to Control622 and higher than NMC111 (Fig. S9). Investigating the excellent rate performance, the lithium-ion diffusion coefficient is measured by CV curves with various scan rates (Fig. S10). The lithium-ion diffu-

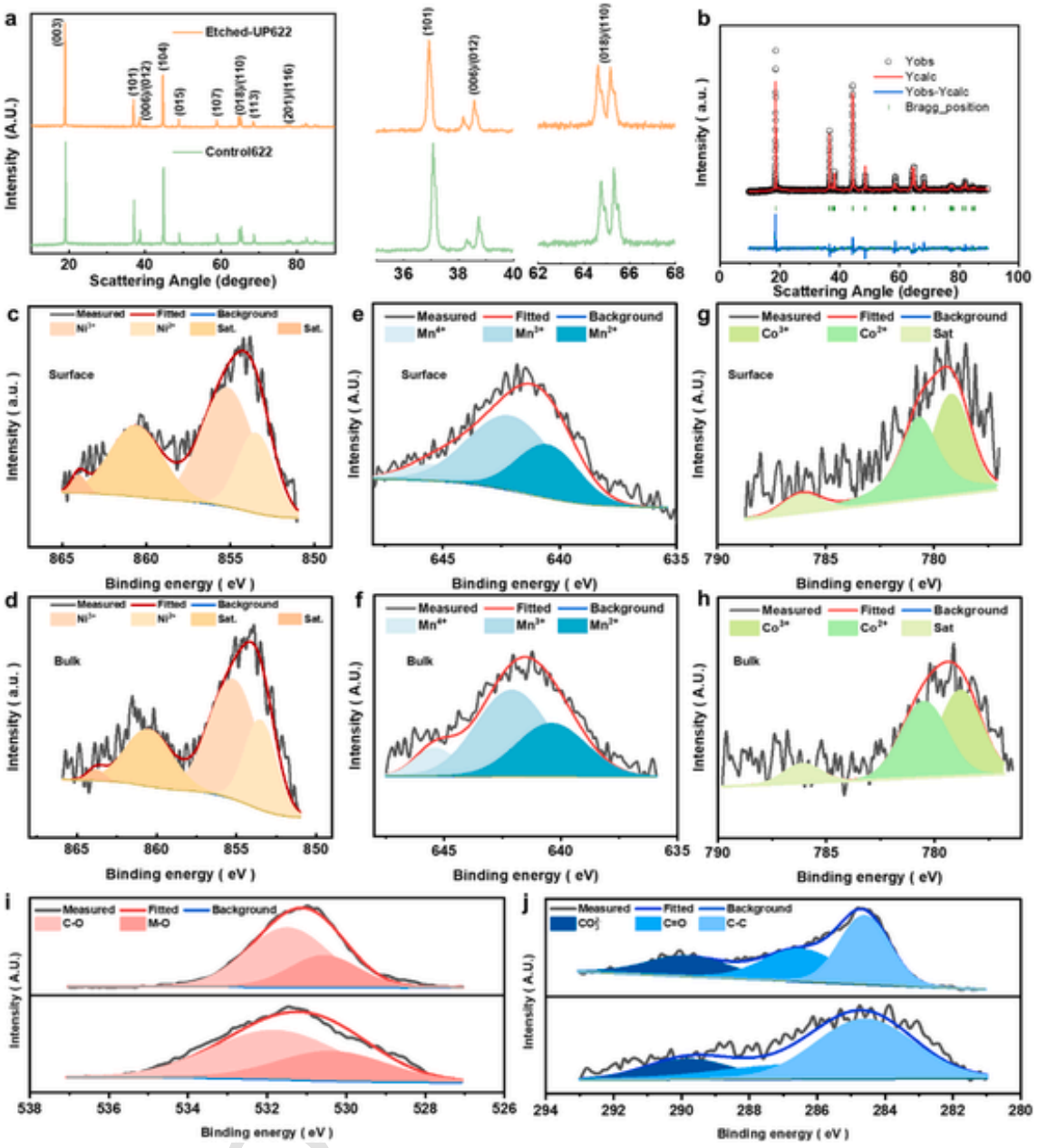

Fig. 4. Properties of Etched-UP622 an Control622. a) XRD pattern of Etched-UP622 and Control622. b) XRD refienment of Control622. c) High-resolution XPS spectra of Ni $2p_{3/2}$ for the surface of Etched-UP622. d) High-resolution XPS spectra of Ni $2p_{3/2}$ for the bulk of Etched-UP622. e) High-resolution XPS spectra of Mn $2p_{3/2}$ for the surface of Etched-UP622. f) High-resolution XPS spectra of Mn $2p_{3/2}$ for the bulk of Etched-UP622. g) High-resolution XPS spectra of Co $2p_{3/2}$ for the surface of Etched-UP622. h) High-resolution XPS spectra of Co $2p_{3/2}$ for the bulk of Etched-UP622. i) High-resolution XPS spectra of O 1s for Control622 and Etched-UP622. j) High-resolution XPS spectra of C 1s for Control622 and Etched-UP622.

sion coefficient of Etched-UP622, Control622, and NMC111 are $6.5*10^{-10}$ cm^2/s, $2.3*10^{-10}$ cm^2/s and $3.0*10^{-12}$ cm^2/s, respectively. The improve lithium-ion diffusion coefficient of Etched-UP622 is due to the short diffusion path enabled by small particle size and enlarged lattice parameters caused by etching process. Due to the high lithium-ion diffusion coefficient, Etched-UP622 delivers superior rate performance than Control622 and NMC111.

Etched-UP622 also delivers better cycle performance than Control622 and NMC111 (Fig. 5d and e). The cycle performance was tested at 2C between 2.5 and 4.3V. The capacity retention of Etched-UP622 is 87.85 % after 100 cycles and 82.32 % after 150 cycles, outperforming Control622 (84.13 % after 100 cycles and 77.54 % after 150 cycles). Additionally, Etched-UP622 delivered highest specific capacities throughout the cycling process (Fig. 5e). As shown in Fig. 5f and g, the specific capacity of Etched-UP622 is 164.9 mAh/g at the first cycle and after 150 cycles, the specific capacity still can reach 135.5 mAh/g, only 29.4 mAh/g was lost during cycling. For Control622, the specific capacity of Control622 is 147.4 mAh/g at the first cycle and after 150 cycles, the specific capacity still can reach 114.3 mAh/g, about 33.2 mAh/g was lost during cycling. Meanwhile, the cycle performance and specific capacity of Etched-UP622 are also higher than NMC111 (Fig. 5d and e and Fig.S11).

Phase transitions during cycling were represented by the dQ/dV profiles (Fig. 5h and i). The voltage shift of the characteristic peak dur-

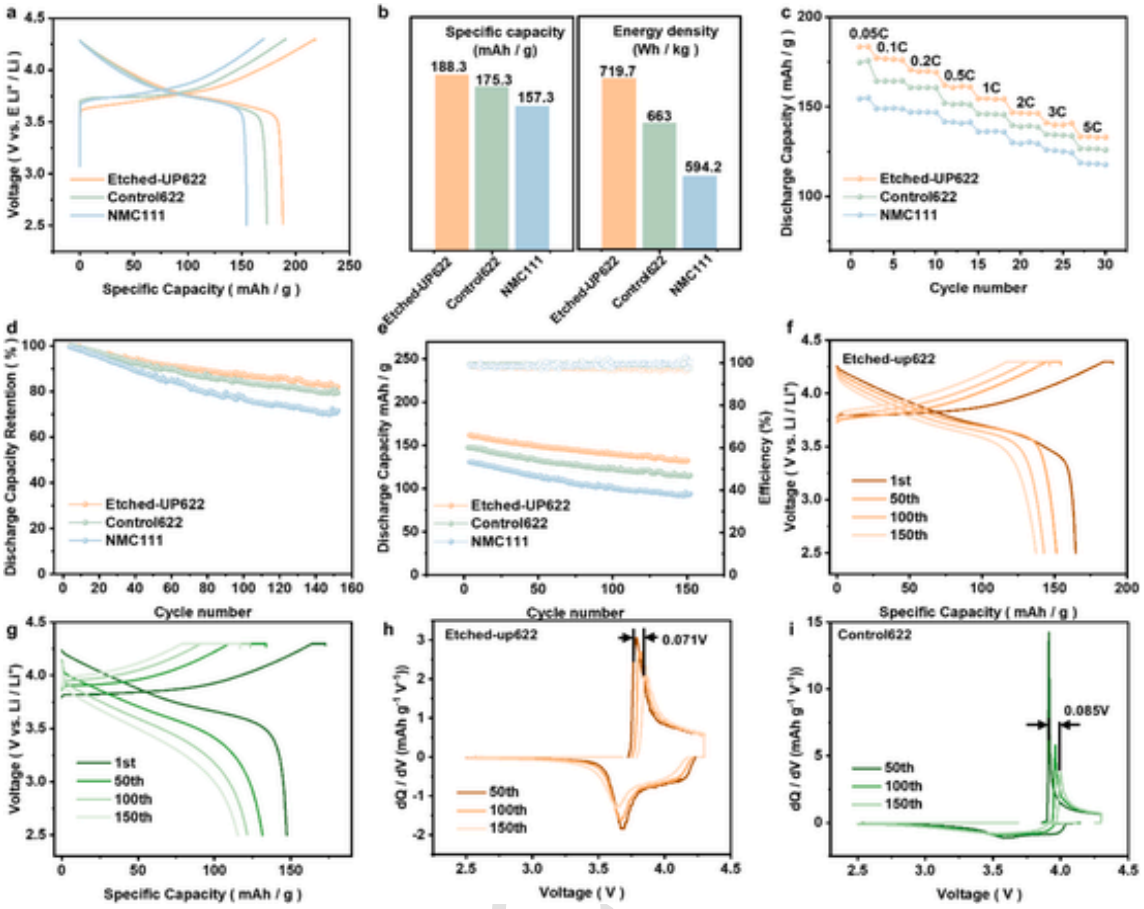

Fig. 5. Electrochemical performance of Etched-622, Control622 and NMC111. a) Initial charge-discharge profiles at 0.05C; b) specific discharge capacity and energy density at 0.05C; c) rate performance; d) capacity retention at 2C; e) cycle performance at 2C of Etched-622, Control622 and NMC111; the capacity voltage curves with different cycle number of f) Etched-622 and g) Control622; differential capacity (dQ/dV) versus voltage profiles with different cycle number of h) Etched-622 and i) Control622.

ing 150 cycles in Control622 was 0.085 V, 19.7 % higher than that observed in Etched-UP622 (0.071 V). This smaller peak shift in Etched-UP622 indicates improved reversibility of the H2 to H3 phase transition during cycling, which contributes to the preservation of mechanical integrity and retention of specific discharge capacity. Additionally, Etched-UP622 also showed a lower voltage shift than NMC111, confirming its superior structural reversibility (Fig. 5h and Fig. S12). EIS results further demonstrated that Etched-UP622 had a smaller semicircle in the Nyquist plots compared to both Control622 and NMC111, reflecting reduced charge transfer resistance during cycling (Figs. S13 and S14, and Table S4).

To further evaluate the cycle performance of Etched-UP622, the cycle performance of Etched-UP622 and Control622 was also tested by full cells (Fig. S15). Anode materials are graphite, and the n/p ratio is between 1.10 and 1.20. The full cells are tested between 2.8 and 4.2V. In the initial charge and discharge curves, the charge capacity of Etched-UP622 and Control622 are 216.4 mAh/g and 201.3 mAh/g, respectively (Fig. S15a). Meanwhile, the discharge capacity of Etched-UP622 and Control622 are 188.4 mAh/g and 176.5 mAh/g, respectively. Therefore, the initial charge and discharge capacity of Etched-UP622 and Control622 is comparable to that of half cells. Additionally, the discharge capacity of Etched-UP622 is 151.5 mAh/g, higher than that of Control622 (137.5 mAh/g). During cycling, the discharge capacity of Etched-UP622 and Control622 did not decrease during the first 37 cycles, but the discharge capacity of Etched-UP622 is always higher than Control622 (Fig. S15b).

Therefore, the electrochemical performance of Etched-UP622 is better than both Control622 and NMC111, confirming its high quality and suitability for commercial applications. Comparison with reported articles about upcycling NMC111 to NMC622, Etched-UP622 delivered the highest discharge capacity (Table S5), indicating the high quality. Meanwhile, our method only includes two steps: etching and sintering, the fewest among all reported methods (Table S5).

3.5. Further studies about upcycling NMC111 to NMC811

In addition to upcycling NMC111 to NMC622, our method also can synthesize cathodes with higher Ni content, like NMC811(Etched-UP811). Etched-UP811 are single crystal particles with some agglomerations and the element distribution in Etched-UP811 is homogeneous (Fig. S16). The composition of Etched-UP811 was tested by ICP (Table S2) and is determined as $Li_{1.02}Ni_{0.82}Mn_{0.09}Co_{0.09}O_2$. Meanwhile, the crystal structure of Etched-UP811 is studied by XRD refinement (Figs. S17 and S18, and Table S1) and XRD (Fig. S14). According to the XRD refinement results, Etched-UP811 delivers comparable lattice parameter and cation mixing to Etched-UP622(Table S1). Meanwhile, Etched-UP811 delivers a single-phase α-$NaFeO_2$ layered structure with distinct (006)/(102) and (018)/(110) peak splitting (Fig. S19). Due to the homogeneous element distribution and well layer structure, the electrochemical performance of Etched-UP811 is comparable to Control811. In the first cycle (Fig. S20), the initial discharge capacity of Etched-UP811 is 192.9 mAh/g, lightly lower than that of Control811 (199.5

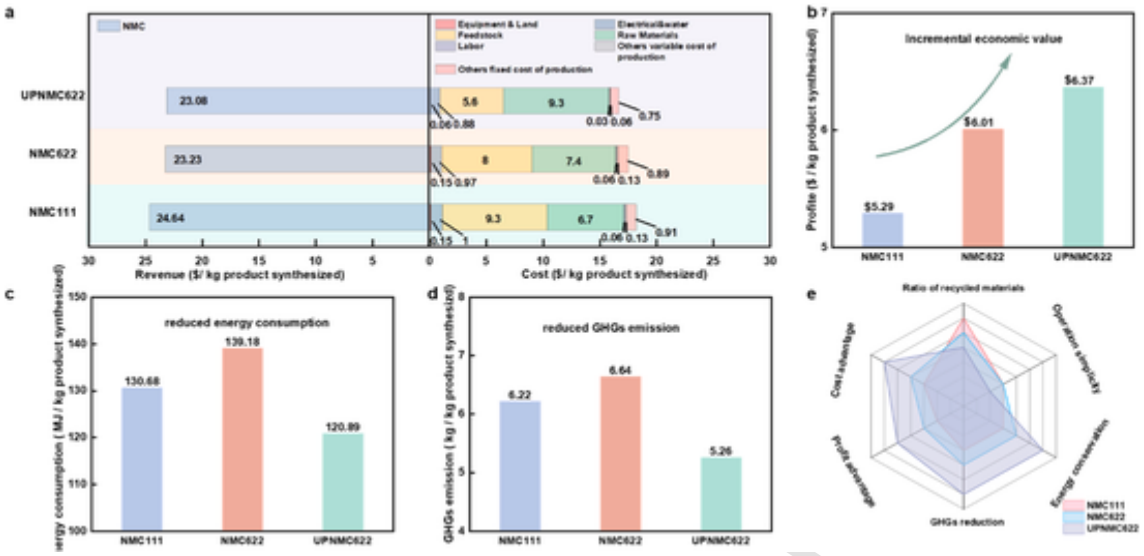

Fig. 6. a) cost and revenue comparison results, b) profit comparison, c) total energy consumption, d) greenhouse gas (GHGs) emission, e) comprehensive comparison of the process for transferring polycrystal NMC111 to single crystal NMC111, transferring polycrystal NMC622 to single crystal NMC622, and upcycling polycrystal NMC111 to single crystal NMC622.

mAh/g). As for rate performance, discharge capacity of Etched-UP811 is 192.9 mAh/g, 188.3 mAh/g, 182.9 mAh/g, 173.8 mAh/g, 166.9 mAh/g, 156.7 mAh/g at 0.05C, 0.1C, 0.2C, 0.5C, 1C, and 2C (Fig. S21). The discharge capacity of Control811 is 199.5 mAh/g, 191.9 mAh/g, 179.1 mAh/g, 164.2 mAh/g, 153.2 mAh/g, 138.8 mAh/g at 0.05C, 0.1C, 0.2C, 1C, and 2C (Fig. S21). However, the electrochemical performance of Etched-UP811 at low rate is still not high enough and the properties of Etched-UP811 should be further optimized.

3.6. Cost analysis

The techno-economic analysis (TEA) of these recycling technologies was performed using the EverBatt 2023 model, comparing the process for transferring polycrystal NMC111 to single crystal NMC111 [29], transferring polycrystal NMC622 to single crystal NMC622 [29], and upcycling polycrystal NMC111 to single crystal NMC622(Figs. S22–S27 and Tables S6–S8). Fig. 6a compares costs and revenues among the three processes. To produce 1 kg single crystal NMC, only the feedstock usage of UPNMC622 is only $5.6, almost half of others. For the proposed upcycling process, 1 mol feedstock can produce 1.65 mol final product while for other process, 1 mol feedstock can produce 1 mol final product. The upcycling process also delivers the highest profit (Fig. 6b). To produce 1 kg single crystal NMC cathode materials, the upcycling process can earn $6.37, 6 % higher than the process of NMC622 and 23 % than the process of NMC111. Meanwhile, the upcycling process also delivers less energy consumption and GHGs emission than other processes (Fig. 6c and d), indicating that the upcycling process is energy-efficient and environmentally friendly. Therefore, as shown in Fig. 6e, our proposed upcycling process delivers more cost advantages, higher profit advantages, reduced GHGs emission, and less energy consumption than other methods, delivering excellent balance between economic and environmental impacts.

4. Conclusion

In this work, we successfully developed a novel etching-assisted upcycling strategy for converting Ni-lean PC NMC111 into Ni-rich single-crystal NMC622 cathode materials. The designed etching process effectively reduced the particle size, transforming PC NMC111 into single-crystal particles, and simultaneously depositing amorphous nickel acetate onto the cathode surface. This structural modification significantly shortened the diffusion pathways, promoting efficient and uniform elemental diffusion during high temperature sintering. Etched-UP622 showed a well-ordered layered structure, large lattice parameters, and substantially low cation mixing. Moreover, the homogeneous elemental distribution in Etched-UP622 further improved electrochemical performance. Remarkably, the energy density of Etched-UP622 can reach 719.7 Wh/kg, 56.7 Wh/kg higher than that of Control622 and 125.5 Wh/kg higher than that of NMC111. Compared with previous reports, our method prevents the requirement of pretreatment and post-treatment. Meanwhile, the discharge capacity of Etched-UP622 delivers higher discharge capacity than other cathode materials with the same composition. Furthermore, this upcycling strategy can be extended to synthesize high-Ni content cathodes, such as NMC811, and provides a practical route toward synthesizing high-performance cathodes through upcycling spent LIBs, facilitating broader industrial implementation and contributing to the circular economy of LIBs. There are also some drawbacks of upcycled cathode materials in terms of particle size and uniformity. To address these issues, molten salt systems such as $LiOH\text{-}LiNO_3$ can be employed to promote metal ion diffusion and regulate particle growth, thereby generating larger and more uniform NMC particles. Meanwhile, to improve the economic value and scalability, future work will focus on exploring cost-effective etching agents and industrial-scale processes.

CRediT authorship contribution statement

Zifei Meng: Writing – review & editing, Writing – original draft, Visualization, Validation, Methodology, Investigation, Formal analysis, Data curation. **Xiaotu Ma:** Methodology, Investigation, Formal analysis, Data curation. **Jiahui Hou:** Writing – review & editing, Visualization, Investigation, Data curation. **Hao Zhou:** Writing – review & editing, Visualization, Investigation, Data curation. **Zexin Wang:** Data curation. **Zeyi Yao:** Writing – review & editing, Visualization, Investigation, Data curation. **Wenting Jin:** Data curation. **Jinzhao Fu:** Data curation. **Zhenzhen Yang:** Data curation. **Adam Shenk:** Data curation. **Yifan Zhang:** Data curation. **Yu Zhong:** Data curation. **Yan Wang:** Writing – review & editing, Validation, Supervision, Re-

sources, Project administration, Methodology, Funding acquisition, Conceptualization.

Declaration of competing interest

The authors declare no conflict of interest.

Acknowledgements

This work was performed through the ReCell Center, which gratefully acknowledge the support from the U.S. Department of Energy (DOE), Office of Energy Efficiency and Renewable Energy, and the Vehicle Technologies Office. XPS work was conducted at the Post Test Facility of Argonne National Laboratory, operated for DOE Office of Science by UChicago Argonne, LLC, under contract no. DE-AC02-06CH11357.

Data availability

Data will be made available on request.

Appendix A. Supplementary data

Supplementary data to this article can be found online at https://doi.org/10.1016/j.jpowsour.2025.238850.

References

[1] Z. Zhang, C. Qin, X. Cheng, J. Li, Y. Zhang, W. Zhao, L. Wang, Y. Du, M. Sui, P. Yan, Electron energy levels determining cathode electrolyte interphase formation, Electron 1 (2023) e9, https://doi.org/10.1002/elt2.9.

[2] Z. Liang, C. Cai, G. Peng, J. Hu, H. Hou, B. Liu, S. Liang, K. Xiao, S. Yuan, J. Yang, Hydrometallurgical recovery of spent lithium ion batteries: environmental strategies and sustainability evaluation, ACS Sustain. Chem. Eng. 9 (2021) 5750–5767, https://doi.org/10.1021/acssuschemeng.1c00942.

[3] J. Hou, Z. Meng, X. Ma, Z. Wang, J. Kim, Z. Yang, J. Wen, M. Sultanov, M. Akin, M. Thakur, Y. Wang, Upcycling mixed spent Ni-Lean cathodes into Ni-Rich polycrystalline cathodes, Energy Storage Mater. 80 (2025) 104386, https://doi.org/10.1016/j.ensm.2025.104386.

[4] Z. Meng, X. Ma, J. Hou, Y. Zheng, Y. Wang, Impurity impacts of recycling NMC cathodes, Adv. Energy Mater. n/a 2405383.https://doi.org/10.1002/aenm.202405383.

[5] A. Manthiram, A reflection on lithium-ion battery cathode chemistry, Nat. Commun. 11 (2020) 1550, https://doi.org/10.1038/s41467-020-15355-0.

[6] F. Xin, A. Goel, X. Chen, H. Zhou, J. Bai, S. Liu, F. Wang, G. Zhou, M.S. Whittingham, Electrochemical characterization and microstructure evolution of Ni-Rich layered cathode materials by Niobium coating/substitution, Chem. Mater. 34 (2022) 7858–7866.

[7] J. Wu, L. Xiao, L. Shen, J.-J. Ran, H. Zhong, Y.-R. Zhu, H. Chen, Recent advancements in hydrometallurgical recycling technologies of spent lithium-ion battery cathode materials, Rare Met. 43 (2024) 879–899, https://doi.org/10.1007/s12598-023-02437-3.

[8] S.-L. Song, R.-Q. Liu, M.-M. Sun, A.-G. Zhen, F.-Z. Kong, Y. Yang, Hydrometallurgical recovery of lithium carbonate and iron phosphate from blended cathode materials of spent lithium-ion battery, Rare Met. 43 (2024) 1275–1287, https://doi.org/10.1007/s12598-023-02493-9.

[9] A.L. Sidiq, O. Floweri, J. Karunawan, O.B. Abdillah, S.P. Santosa, F. Iskandar, NCM cathode active materials reproduced from end-of-life Li-ion batteries using a simple and green hydrometallurgical recycling process, Mater. Res. Bull. 153 (2022) 111901, https://doi.org/10.1016/j.materresbull.2022.111901.

[10] C. Pan, Y. Shen, Pyrometallurgical recycling of spent lithium-ion batteries from conventional roasting to synergistic pyrolysis with organic wastes, J. Energy Chem. 85 (2023) 547–561, https://doi.org/10.1016/j.jechem.2023.06.040.

[11] J. Fan, H. Luo, T. Wang, S. Dai, Progress in direct recycling of spent lithium nickel manganese cobalt oxide (NMC) cathodes, Energy Storage Mater. 73 (2024) 103813, https://doi.org/10.1016/j.ensm.2024.103813.

[12] A.D.A. Bin Abu Sofian, S.R. Majid, K. Kang, J.-K. Kim, P.L. Show, Upcycling and recycling of spent battery waste for a sustainable future: progress and perspectives, Prog. Mater. Sci. 153 (2025) 101478, https://doi.org/10.1016/j.pmatsci.2025.101478.

[13] P. Xu, D.H.S. Tan, B. Jiao, H. Gao, X. Yu, Z. Chen, A materials perspective on direct recycling of lithium-ion batteries: principles, challenges and opportunities, Adv. Funct. Mater. 33 (2023) 2213168, https://doi.org/10.1002/adfm.202213168.

[14] G. Harper, R. Sommerville, E. Kendrick, L. Driscoll, P. Slater, R. Stolkin, A. Walton, P. Christensen, O. Heidrich, S. Lambert, A. Abbott, K. Ryder, L. Gaines, P. Anderson, Recycling lithium-ion batteries from electric vehicles, Nature 575 (2019) 75–86, https://doi.org/10.1038/s41586-019-1682-5.

[15] X. Ma, Z. Meng, M.V. Bellonia, J. Spangenberger, G. Harper, E. Gratz, E. Olivetti, R. Arsenault, Y. Wang, The evolution of lithium-ion battery recycling, Nat. Rev. Clean Technol. 1 (2025) 75–94, https://doi.org/10.1038/s44359-024-00010-4.

[16] S. Natarajan, S. Noda, Advancements in direct recycling technologies for lithium-ion battery cathodes: overcoming challenges in cathode regeneration, Mater. Sci. Eng. R Rep. 164 (2025) 100976, https://doi.org/10.1016/j.mser.2025.100976.

[17] Y.S. Byeon, H.B. Lee, Y. Hong, H.-s. Kim, Y.-J. Kim, W. Cho, M.-S. Park, Cation-deficient LixWO3 surface coating on Ni-Rich cathodes materials for lithium-ion batteries, ACS Appl. Mater. Interfaces 17 (2025) 9322–9331, https://doi.org/10.1021/acsami.4c18935.

[18] K. Chen, W. Cai, Z. Hu, Q. Huang, A. Wang, Z. Zeng, J. Song, Y. Sun, Q. Kong, W. Feng, T. Chen, Z. Wu, Y. Song, X. Guo, Damage mechanisms and recent research advances in Ni-rich layered cathode materials for lithium-ion batteries, Electron 2 (2024) e27, https://doi.org/10.1002/elt2.27.

[19] G. Qian, Z. Li, Y. Wang, X. Xie, Y. He, J. Li, Y. Zhu, S. Xie, Z. Cheng, H. Che, Y. Shen, L. Chen, X. Huang, P. Pianetta, Z.-F. Ma, Y. Liu, L. Li, Value-creating upcycling of retired electric vehicle battery cathodes, Cell Rep. Phys. Sci. 3 (2022) 100741, https://doi.org/10.1016/j.xcrp.2022.100741.

[20] S. Wang, G. Tan, W. Li, S. Yang, Y. Lu, Y.-F. Huang, W. Wang, Y. Wang, C. Xu, Influence of nickel-content and cycling rate on the phase behavior of layered nickel-rich cathode materials for lithium-ion batteries, ACS Appl. Mater. Interfaces 17 (2025) 21122–21132, https://doi.org/10.1021/acsami.4c21038.

[21] Y. Wang, C. Yuan, Direct upcycling of degraded NCM via low-temperature surface engineering for high performance lithium-ion batteries, EES Batter. (2025), https://doi.org/10.1039/D5EB00018A.

[22] X. Ma, J. Hou, P. Vanaphuti, Z. Yao, J. Fu, L. Azhari, Y. Liu, Y. Wang, Direct upcycling of mixed Ni-lean polycrystals to single-crystal Ni-rich cathode materials, Chem.8 (2022) 1944–1955.

[23] E. Allen, J. Macholz, M. Nisbet, N. Chowdhury, F. Wang, M. Porwal, D.T. Keane, W. Guise Jr., Z. Dundek, M. Caple, V. Nikitin, J. Cabana, Q. Dai, A. Lipson, Cathode upcycling for direct recycling of lithium-ion batteries using a precipitation approach, Adv. Energy Mater. n/a 2500699.https://doi.org/10.1002/aenm.202500699.

[24] N. Zhang, H. Li, C. Ye, S.-Z. Qiao, Mechanical homogenization promoting dual-directional upcycling of layered oxide cathodes, Adv. Mater. n/a 2504380.https://doi.org/10.1002/adma.202504380.

[25] H. Gao, Q. Yan, D. Tran, X. Yu, H. Liu, M. Li, W. Li, J. Wu, W. Tang, V. Gupta, J. Luo, Z. Chen, Upcycling of spent LiNi0.33Co0.33Mn0.33O2 to single-crystal Ni-Rich cathodes using lean precursors, ACS Energy Lett. 8 (2023) 4136–4144, https://doi.org/10.1021/acsenergylett.3c01454.

[26] K.I. Hamad, Y. Xing, Stabilizing Li-rich NMC materials by using precursor salts with acetate and nitrate anions for Li-ion batteries, Batteries 5 (2019) 69, https://doi.org/10.3390/batteries5040069.

[27] Z.-w. Xiao, Y.-j. Zhang, Y.-f. Wang, Synthesis of high-capacity LiNi0.8Co0.1Mn0.1O2 cathode by transition metal acetates, Trans. Nonferrous Metals Soc. China 25 (2015) 1568–1574, https://doi.org/10.1016/S1003-6326(15)63759-1.

[28] J.D. Desai, S.-K. Min, K.-D. Jung, O.-S. Joo, Spray pyrolytic synthesis of large area NiOx thin films from aqueous nickel acetate solutions, Appl. Surf. Sci. 253 (2006) 1781–1786, https://doi.org/10.1016/j.apsusc.2006.03.009.

[29] X. Ma, P. Vanaphuti, J. Fu, J. Hou, Y. Liu, R. Zhang, S. Bong, Z. Yao, Z. Yang, Y. Wang, A universal etching method for synthesizing high-performance single crystal cathode materials, Nano Energy 87 (2021), https://doi.org/10.1016/j.nanoen.2021.106194.

[30] M. Zybert, H. Ronduda, A. Ostrowski, K. Sobczak, D. Moszyński, W. Raróg-Pilecka, B. Hamankiewicz, W. Wieczorek, Structural analysis and electrochemical investigation of dual-doped NMC622 cathode material: effect of sodium and neodymium on the performance in Li-ion batteries, Energy Rep. 10 (2023) 1238–1248, https://doi.org/10.1016/j.egyr.2023.07.061.

[31] G. Qian, Y. Zhang, L. Li, R. Zhang, J. Xu, Z. Cheng, S. Xie, H. Wang, Q. Rao, Y. He, Y. Shen, L. Chen, M. Tang, Z.-F. Ma, Single-crystal nickel-rich layered-oxide battery cathode materials: synthesis, electrochemistry, and intra-granular fracture, Energy Storage Mater. 27 (2020) 140–149, https://doi.org/10.1016/j.ensm.2020.01.027.

[32] Z. Meng, J. Hou, P. Thanwisai, J. Fu, Z. Yao, Y. Zheng, W. Jin, Z. Wang, Z. Yang, X. Ma, Y. Wang, Understanding the effects of Bi modification on the properties of Ni-Rich cathodes, Batter. Supercaps 7 (2024) e202400107, https://doi.org/10.1002/batt.202400107.

[33] R. Zhang, Z. Meng, X. Ma, M. Chen, B. Chen, Y. Zheng, Z. Yao, P. Vanaphuti, S. Bong, Z. Yang, Y. Wang, Understanding fundamental effects of Cu impurity in different forms for recovered LiNi0.6Co0.2Mn0.2O2 cathode materials, Nano Energy 78 (2020) 105214, https://doi.org/10.1016/j.nanoen.2020.105214.

[34] H.-x. Wei, L.-b. Tang, Y.-d. Huang, Z.-y. Wang, Y.-h. Luo, Z.-j. He, C. Yan, J. Mao, K.-h. Dai, J.-c. Zheng, Comprehensive understanding of Li/Ni intermixing in layered transition metal oxides, Mater. Today (2021), https://doi.org/10.1016/j.mattod.2021.09.013.

[35] A. Ran, S. Chen, M. Cheng, Z. Liang, B. Li, G. Zhou, F. Kang, X. Zhang, G. Wei, A single-crystal nickel-rich material as a highly stable cathode for lithium-ion batteries, J. Mater. Chem. A. 10 (2022) 19680–19689.

[36] X. Ren, L. Zou, X. Cao, M.H. Engelhard, W. Liu, S.D. Burton, H. Lee, C. Niu, B.E. Matthews, Z. Zhu, C. Wang, B.W. Arey, J. Xiao, J. Liu, J.-G. Zhang, W. Xu, Enabling high-voltage lithium-metal batteries under practical conditions, Joule 3 (2019) 1662–1676, https://doi.org/10.1016/j.joule.2019.05.006.

[37] L. Yu, J. Wang, T. Zhou, W. Huang, T. Li, L. Ma, X. Xiao, S.-B. Son, S.N. Ehrlich, J. Wen, K. Amine, T. Liu, Unraveling the origin of air-stability in single-crystalline layered oxide positive electrode materials, Nat. Commun. 16 (2025) 6519, https://

doi.org/10.1038/s41467-025-61304-0.